

*Submitted: ApJ, April 4, 2010; Revised May 11, 2010*

# A Physically-Based Method for Scaling Cepheid Light Curves for Future Distance Determinations

Wendy L. Freedman & Barry F. Madore

*The Observatories  
Carnegie Institution for Science  
813 Santa Barbara St.  
Pasadena, CA 91101*

wendy@obs.carnegiescience.edu, barry@obs.carnegiescience.edu

## **ABSTRACT**

We present a technique for decomposing Cepheid light curves into their fundamental constituent parts; that is, their radius and temperature variations. We demonstrate that any given pair of optical luminosity and color curves can be used to predict the shape, amplitude and phase of a Cepheid's light variation at any other wavelength. With such predictions in hand, a single new observation at any given new wavelength can be used to normalize the properties of the predicted light curve, and in specific, derive a precise value of the time-averaged mean. We suggest that this method will be of great advantage in efficiently observing and precisely obtaining the mean properties of known Cepheids scheduled to be observed at new wavelengths, specifically in the mid-infrared where JWST will be operating.

*“The variable star  $\delta$  Cephei, the prototype of its class, has been observed so long and so often – visually, photographically, and photoelectrically – that little new can be expected from additional observations, no matter what their quality.”* – Stebbins (1945)

## 1. Introduction

The absolute luminosities of stars can be simply expressed as the product of only two quantities: the total area of the radiating surface and the mean surface brightness of that same area. For spherical stars the area is readily calculated from the radius; and the surface brightness is locally controlled by the temperature. For a radially pulsating star, such as a Cepheid, its time variation in luminosity is also controlled by the coupled time variation of those same two physical parameters, radius and temperature. In this paper, we explore this property further, enabling us to use data obtained at multiple wavelengths to provide constraints on these parameters.

The basic relations are captured by Stefan’s Law in the definition of the effective temperature ( $T_e$ ) and its derivative. Bolometrically

$$L = 4\pi R^2 \sigma T_e^4$$

and

$$\Delta L/L = 2\Delta R/R + 4\Delta T_e/T_e + constant$$

The differential form clearly demonstrates that the luminosity variation should be readily decomposed into two terms, a radius and a temperature term. Since the temperature of a star is readily estimated from its (optical) colors, it follows that the surface area variation must be whatever residual remains after the color variation is scaled (to a surface brightness) and subtracted from the (composite) luminosity curve. This suggests a path whereby the two physical terms can be decoupled empirically and evaluated independently.

The above equations apply to the bolometric luminosity. Does this simplicity transfer over to empirically measured broad-band photometry? At first sight, multi-wavelength observations (of Cepheids in particular) might suggest that the situation is far more complicated, given that Cepheid light curves at different wavelengths have fundamentally different shapes, systematically changing amplitudes and advancing phases of maximum light as a function of wavelength. See Figure 1 for examples.

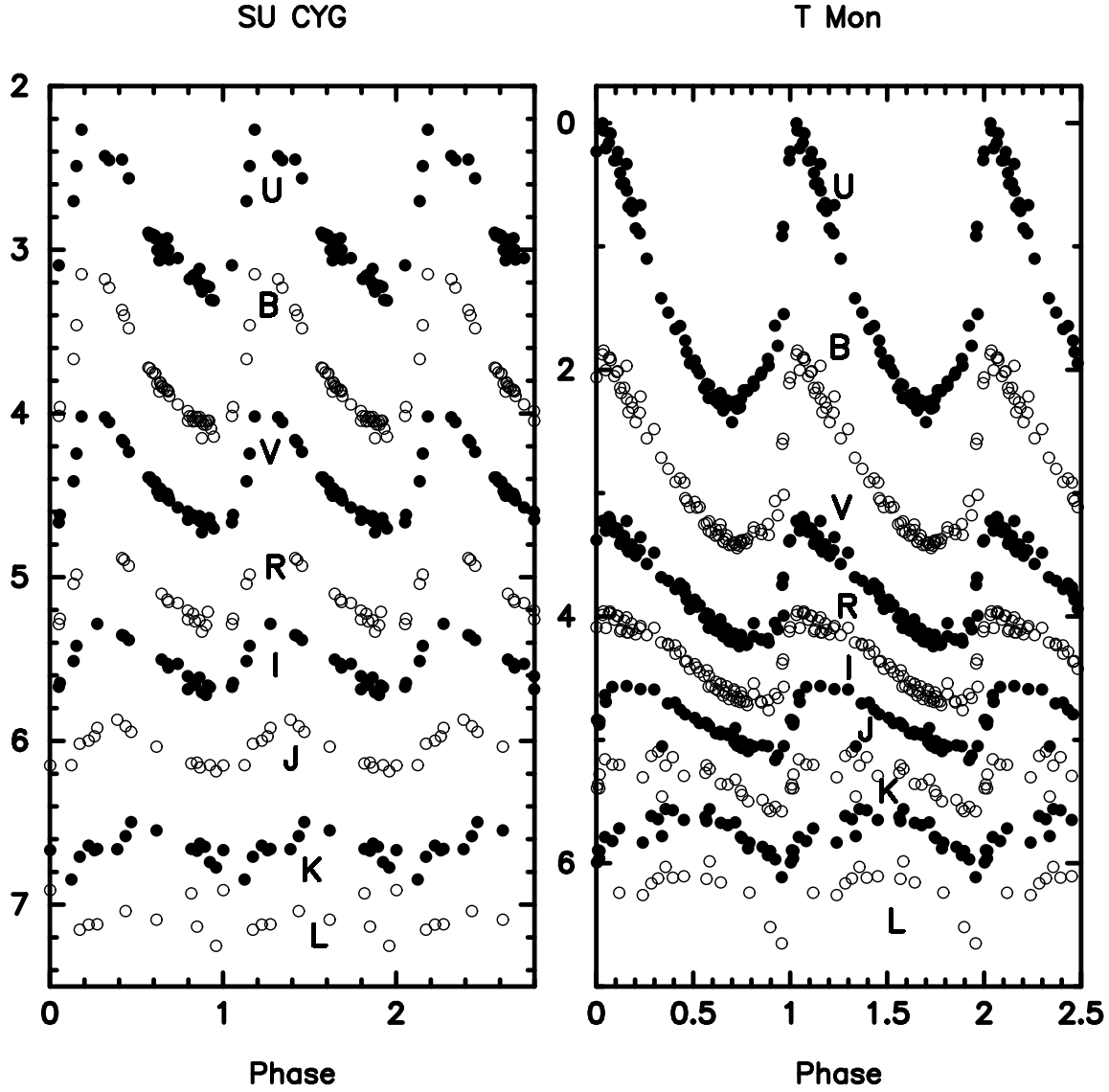


Fig. 1.— Multi-wavelength light curves for two Galactic Cepheids, SU Cyg and T Mon. The run of amplitude and phase of maximum light for Cepheid light curves as a function of wavelength of the observations is easily seen in these data drawn primarily from Wisniewski and Johnson (1968). Moving from top to bottom the amplitudes decrease as the wavelength increases. The phase of maximum light at the progressively longer wavelengths falls systematically behind the timing of maximum light at the shorter wavelengths. Finally, it is quite apparent that the overall shape of the light curve also changes with wavelength. In the blue there is a steep rise followed by a slower, linear decline. In the near infrared the light curve is more symmetric and cycloidal in nature, showing a wide maximum flanked symmetrically by rapid dips to short-lived minima.

Early observers of Cepheids noted that the amplitudes of those variable stars systematically decreased as a function of advancing wavelength (Wisniewski & Johnson 1968), where it was noted that the shapes of Cepheid light curves became less triangular and more cycloidal in form as their amplitudes dropped. It was also seen that the timing of maximum light for Cepheids was shifting to later phases, again as longer and longer wavelengths were explored (see for example the atlas of multi-wavelength light curves in Wisniewski & Johnson). Stebbins (1945) is the first to have noted the decreasing amplitude a Cepheid (by a factor of 3.4 for his observations of  $\delta$  Cep) with increasing wavelength of his observations (from U[3530Å] to I<sub>S</sub>[10,300Å]), and the concomitant shifting of maximum light to later phases (by +0.05 in phase over the same, U to I, wavelength range). The first practical use of these trends was made by Freedman (1988; see below).

The photometric behavior described above can be understood as follows: The asymptotic (long-wavelength) behavior of a Cepheid light curve is dominated by the (geometric) radius variation. It is well known from integrating radial-velocity curves of Cepheids that the form of the radius variation with time is well described as being cycloidal in shape (see, for example, radius and radial velocity data presented by Imbert 1981). Since it is geometric in nature, the contribution of the radius variation to the light curve of a Cepheid will be largely independent of wavelength, modulo small (wavelength-dependent) optical depth effects. If there were no additive temperature variations, any given Cepheid’s light curve would have the same shape at all wavelengths; but observations indicate otherwise. A test can be made by subtracting two light curves obtained at different wavelengths. The differencing directly cancels out the equally-contributing radius term, and then leaves a pure temperature-driven term. At short wavelengths color is primarily driven by temperature. Clearly then, by appropriately scaling the color curve and subtracting it (in magnitude space) from the luminosity curve one will be left with the areal variation (i.e., radius) curve. These same precepts are at the heart of the Baade-Wesselink method, where photometry and radial velocities are combined to determine absolute radii and metric distances. The method we are describing here provides a way of measuring precision distances without the need for radial velocity measurements.

## 2. Extracting Radius Curves from Optical Light Curves

In a study of the Local Group dwarf galaxy, IC 1613, Freedman (1988) showed that one could use well-sampled B-band light curves, for example, to predict the amplitudes at I-band wavelengths, adjust the phasing appropriately, and predict the mean magnitude at I, based on a single observation at that longer wavelength. The scaling relations, rephasing and

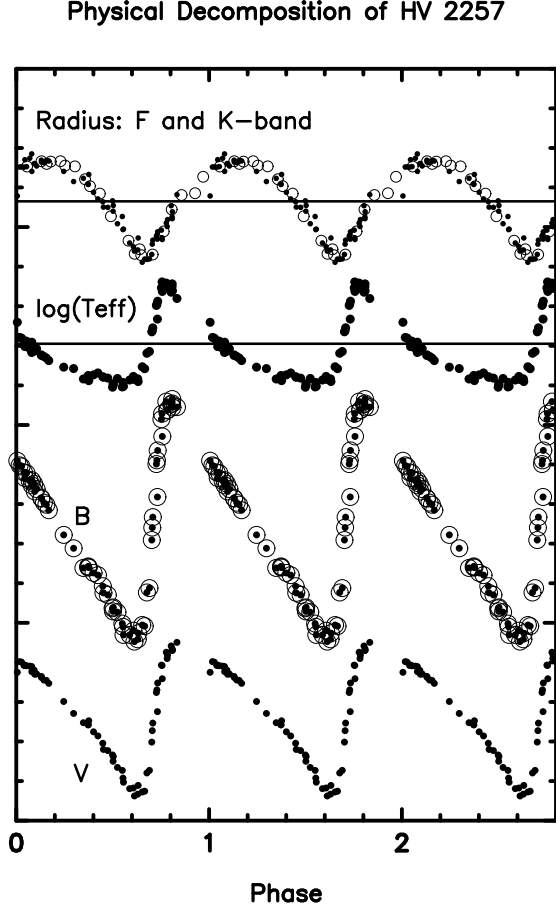


Fig. 2.— An example of the physical decomposition of a Cepheid light curve. The B and V light curves for the Large Magellanic Cloud Cepheid, HV 2257, are shown in the lower part of the plot. They act as the generating functions for the two curves plotted at the top of the figure. The larger filled circles, marked  $\log T_{eff}$ , define the (B-V) color curve. The upper plot is a composite of K-band, near-infrared data (K: open circles), and the CPR predicted radial-displacement curve (F: filled circles) obtained by scaling and subtracting the temperature variation from the observed luminosity curves leaving the radius variation. The similarity in the K and F curves is striking.

predicted light-curve shapes were only approximate, but given the factor of  $2\text{--}3\times$  systematic reduction in amplitude in going from B to I the method provided a significant improvement to the mean magnitudes.

Subsequently, a number of follow-up studies introduced greater degrees of mathematical sophistication, a larger variety of templates (Stetson 1996; Labhardt, Sandage & Tammann 1997) and more complicated fitting procedures, based, for example, on Fourier decomposition (e.g., Ngeow et al. 2003; Soszynski, Gieren & Pietrzynski 2005), principal component analysis (as in Tanvir et al. 2005; Kanbur & Mariani 2004), or a combination of both (Yoachim et al. 2009). Labhardt, Sandage & Tammann concluded that except for a brief period of time, during the ascending phase of the light curve, their method and that of Freedman (1988) had the same precision (see their Figure 2); while Fourier decomposition methods suffer from global fitting instabilities when samples are sparse or highly clumped, and especially when higher-order terms are included. Nevertheless, with care each of the methods is capable of scaling light curves across wavelengths and reducing the scatter in the predicted/fitted mean. All of these methods are phenomenological. In the following we describe a physically-motivated approach, which is simpler and more precise. We refer to this as the Carnegie Photometric Radial-Displacement (CPR) Method.

### 3. The Carnegie Photometric Radial-Displacement (CPR) Method

Scaling and subtracting the temperature variation to reveal the pure radius variations was first discussed by Madore (1985) while attempting to produce a function that was minimally impacted by phase. The so-called Feinheit function combines the luminosity and color in such a way so as to minimize the amplitude of the resulting light variation. This function,  $F = V - \alpha \times (B - V)$ , reaches a minimum amplitude when the temperature variation is cancelled, leaving only the radius variation contributing to the light variation. As it turns out the color coefficient “ $\alpha$ ” in the definition of the Feinheit function is directly related to “ $a$ ” in the Baade-Wesselink formalism used in calculating the logarithmic surface brightness from colors (for example, see Kervella et al. 2004 for a recent application and compilation). The Feinheit function then is numerically equivalent to the so-called “photometric radial displacement”. The values of the Feinheit color coefficients “ $\alpha$ ” statistically correlate with period (see Figure 3 in Madore 1985). It is reasonably expected that they are physically controlled by temperature (i.e., more directly correlated with intrinsic color.)

In Figure 2 we first demonstrate the physical decomposition of an optical light curve into its temperature and radius components. We begin with the B and V light curves as plotted in the lower portion of the figure. We note the larger amplitude of the B-band light curve as

Photometric Velocity Curve for HV 2257

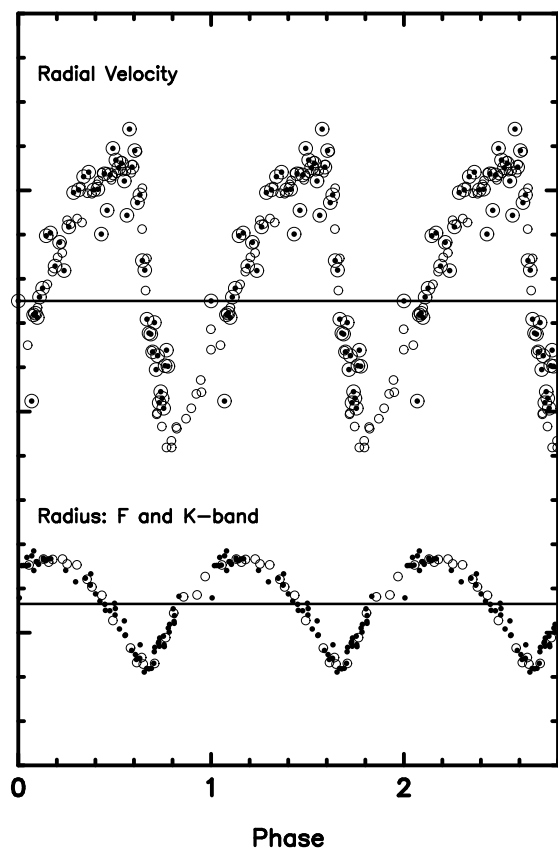


Fig. 3.— A demonstration that F and K both represent radius variations. Lower plot: The CPR predictions (F: filled circles) overplotted on K-band light curve (K: open circles) for the LMC Cepheid HV 2257, as in Fig. 2. The upper plot shows the published radial velocity curve (open circles, from Imbert et al. 1985; Imbert 1987) with the scaled first derivatives of the CPR data overplotted (circled dots).

compared to V. It is also easily seen, in comparison, that the B-band light curve has much more linear decline than the more rounded descending portion of the V-band light curve. A straightforward, point-by-point differencing of the two light curves results in the color curve plotted just above the B-band light curve. Given that color maps directly to (logarithmic) temperature we have labelled that curve as  $\log(T_{eff})$ . We next scale the  $\log(T_{eff})$  curve and subtract its contribution from the B-band light curve giving rise to the radius curve delineated by the filled circles plotted across the top of the panel. The K-band light curve is widely considered to be dominated by pure radial variations; those data are plotted as open circles in the same portion of the diagram. The coincidence is impressive given that only a vertical shift in the two magnitude scales was allowed.

In Figure 3 we make our final argument for F being identified with the radial displacement. The predicted radius curve (F: filled circles) and the overplotted K-band data (K: open circles) as already given in Figure 2 (above) are reproduced, for convenience, at the bottom of this figure. We then take the first derivative of the K-band light curve and plot it as circled dots in the upper portion of the frame (labeled “Radial Velocity”). Over-plotted in that same part of the frame are published radial velocities for HV 2257 from (Imbert et al. 1985; Imbert 1987). The only adjustment was the amplitude of the variation to match the logarithmic scaling of the photometric data. Below, we quantify the level of this agreement. We conclude that K, F and radius are equivalent representations that allow a successful decomposition of optical light curves into physical quantities.

However, before moving on we offer the following discussion prompted by the kind suggestions made by the referee. Consider the following equations describing the decomposition of the light variation in two distinct bands (B and V, for example) due to areal variations parameterized by  $\theta$  and variations in the surface brightness induced by temperature variations,  $T_{eff}$

$$B = B_0 - 5 \log(\theta) - C_B \times 2.5 \log(T_{eff})$$

$$V = V_0 - 5 \log(\theta) - C_V \times 2.5 \log(T_{eff})$$

Recalling that  $F = V - \alpha(B - V)$  this translates into

$$F = [V_0 - \alpha(B_0 - V_0)] - 5 \log(\theta) - [C_V - \alpha(C_B - C_V)] \times 2.5 \log(T_{eff})$$

So by setting  $\alpha = C_V / (C_V - C_B)$  the Feinheit function (by design) eliminates the temperature variation. If the color-temperature relation is non-linear then the values of  $C_B$  and  $C_V$  will themselves change with temperature and so  $\alpha$  will also be expected to be a function of intrinsic color (i.e., temperature) also. Since longer-period Cepheids are statistically redder (cooler) than short-period Cepheids it follows that  $\alpha$  will also be a (statistical) function



of period, which explains the correlation that was found and reported in Madore (1985), as stated earlier.

We now explore how the CPR method can be used in a practical sense through a series of decomposition and reconstruction examples. These range from Galactic examples with dozens of observations covering half a dozen or more wavelengths, to LMC Cepheids with extensive optical and near-infrared data, to Cepheids at the edge of detectability in more distant galaxies where one or two observations are available beyond their (optical) discovery wavelengths.

We now consider a Galactic Cepheid, YZ Cyg, for a further demonstration of the CPR decomposition and prediction method. This time we use BV data to predict the details of the slightly longer-wavelength light curve in the R band, but this time also to predict the light curve behavior at the shorter U-band wavelength. In the lower panel the published UBVR observations are shown as open circles. At the top of the panel are smoothed versions of the radius variation (as derived only from the BV light curves), and the temperature curve again derived exclusively from the BV light curves. Now immediately above the R-band observations is the predicted (solid line) R-band light curve based on the reprojected radius and temperature curves. Below the U-band data is the (solid line) prediction for the ultraviolet light curve. To the eye they are indistinguishable. We now quantify that match.

In Figure 4 we isolate the R & U-band data and their predictions now showing the point-by-point reprojection of the combined radius and temperature curves back into the observational planes. Below each curve is the run of differences between the observed and the predicted light curves. Because no smoothing in the physical plane was applied, the residuals carry the full complement of the uncorrelated errors associated with all three of the B, V and R (B, V and U) data points that went into the various solutions. The calculated scatter in R-band comparison is  $\pm 0.013$  mag; the scatter in U is  $\pm 0.028$  mag. The  $\pm 2$ -sigma bounds are plotted around the measured differences. There are no significant trends of the scatter with phase. The scatter is consistent with photometric errors in the combined data.

In Figure 5 we show the point-by-point prediction of JH & K light curves from the precision BV CCD data for HV 2257 taken from Mofett et al. (1998). In the lower part of the panel we show the individually phased BV observations folded over 2.8 cycles. Using these observations to produce radius and temperature curves we then reproject these data back into the observational plane but now at the three near-infrared JHK wavelength bands. Those predictions are shown by open circles in the upper part of the panel. Overplotted on the predicted values are the observed JHK data (again as filled circles) from Persson et al. (2004). Figure 6 shows the results of predicting lightcurves at longer (R-band) and shorter (U-band) wavelengths than the basis light curves. To within the observational scatter the

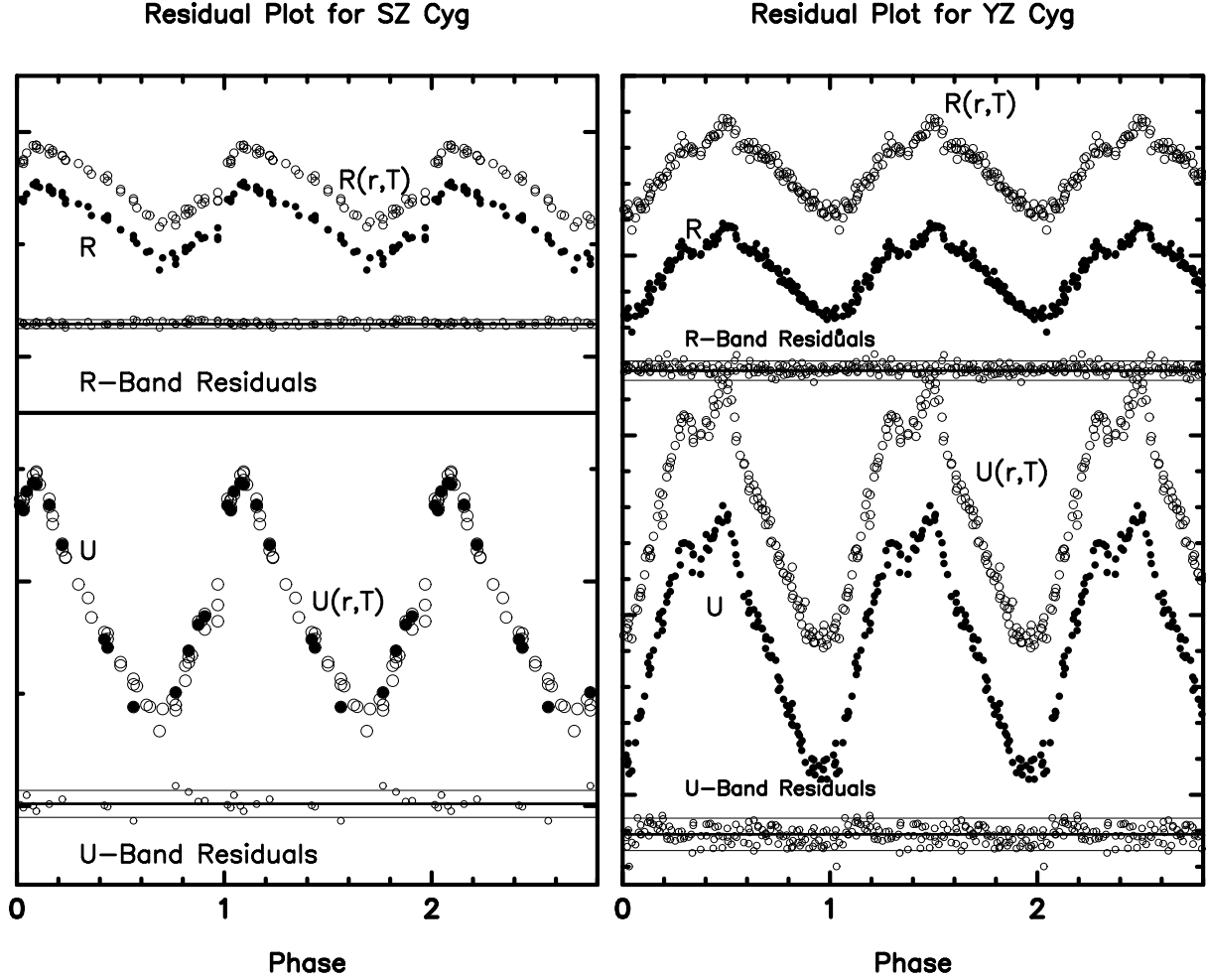


Fig. 4.— Point-by-point CPR reconstructions of the R (upper) and U (lower) light curves based upon predictions from the B and V data alone. The two flat-lined scatter plots below each pair of light curves are the individual differences between the observed and the predicted light curves. No significant change in scatter nor any systematic deviations from zero is seen as a function of phase. To within the scatter of the observations, no further parameter characterizing the light curves is indicated; in fact, the fits are consistent with being dispersionless.

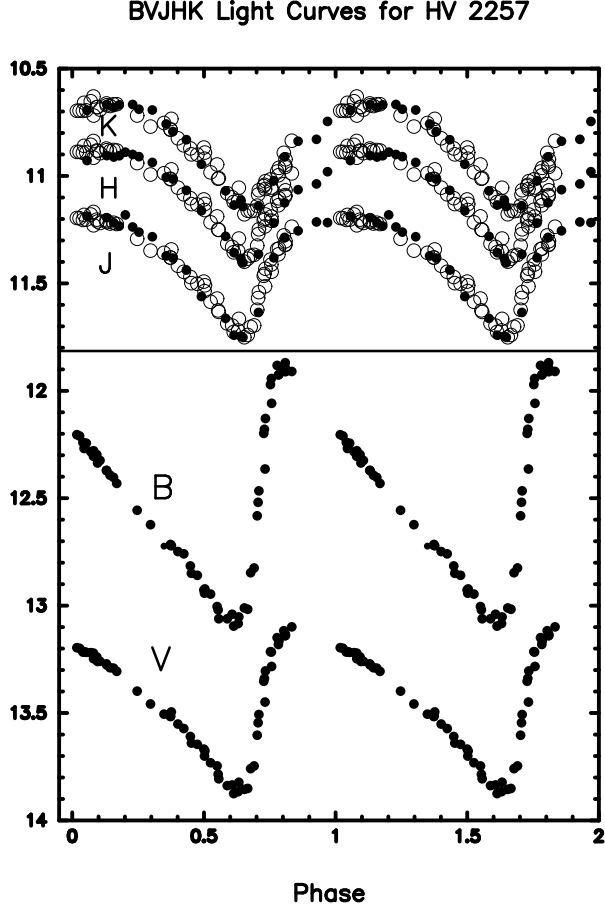


Fig. 5.— Prediction of JHK near-infrared light curves for HV 2257 from BV optical light curves. Open circles in the upper three plots are CPR predictions for the amplitude, shape and phasing of the three near-infrared light curves. The observed data are shown as filled circles. Excellent agreement is seen.

observations and the predictions are indistinguishable.

We close this series of demonstration cases with an example taken from the recent literature on multi-wavelength observations of Cepheids significantly more distant and fainter than our Galactic examples and about 40 times further away than the LMC. This is the Cepheid C15 in the South Polar Group spiral galaxy NGC 300. Plotted as circled circles in the lower half of Figure 7 are V and I data from Gieren et al. (2004). From these two wavelengths we constructed temperature and radius curves, applied the CPR Method and reprojected them into the K and J band passes for which there are random phase data from Gieren et al. (2005). The fit of the predictions to the two observations in each of J and K are shown at the top of the figure. Despite having switched from BV to VI for our physical decomposition basis the method demonstrably works here too in very accurately phasing up with the observed data.

#### 4. Conclusions

We have shown that the diversity of Cepheid lightcurve amplitudes, shapes and relative phases, encountered over all currently available wavelengths, are reducible to two simple but also physically meaningful quantities: radius and temperature. Given a set of applicable scaling relations, the radius and temperature curves can be used to predict the exact form of any given Cepheid’s behavior at all currently observed wavelengths, from the ultraviolet to the mid-infrared (see Figure 8). Given this predictive tool set one can now realize enormous observational gains with no loss in signal-to-noise in extracting mean properties of Cepheids at other wavelengths. This is especially true for deriving time-averaged mean magnitudes and mean colors, derived from sparsely-sampled, random-phase observations at even longer or shorter wavelengths.

The next paper in this series will present and discuss the exact calibration of this method, for future applications especially at mid-infrared wavelengths where JWST will be fully operational.

#### 5. Acknowledgments

We thank the referee for his/her detailed suggestion to make the physical-variable decomposition of the Feinheit formalism more explicit.

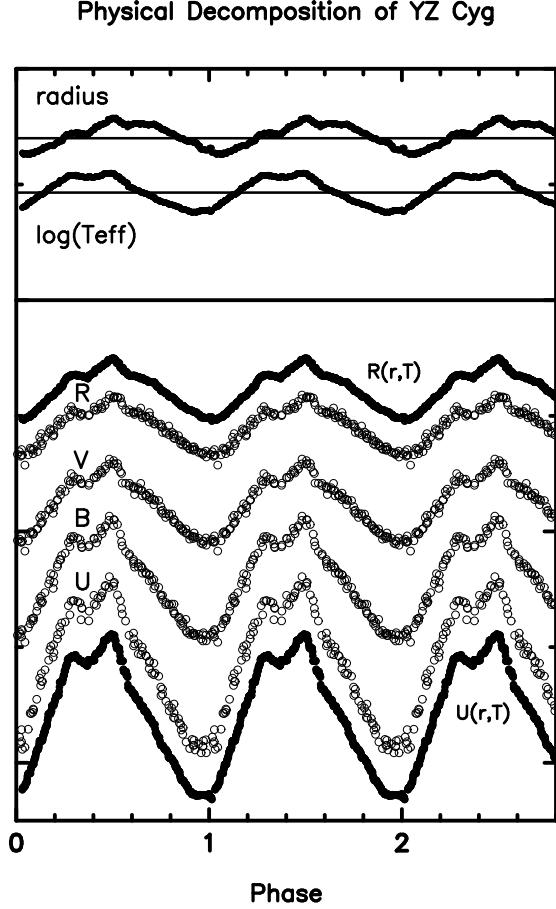


Fig. 6.— UBVR light curves for the Galactic Cepheid YZ Cyg. Open circles are the published data from (Wisniewski & Johnson 1968). At the top of the panel are the smoothed versions of the radius and temperature curves made as intermediary functions in the CPR reconstruction. The solid curves above and below the published-data R & U light curves are the CPR predicted light curves, labeled  $R(r,T)$  and  $U(r,T)$ , respectively. Because of the precision of the predictions the two curves (predicted and observed) are displaced so that the data points and the predictions can be seen separately; if over-plotted the points would be indistinguishable.

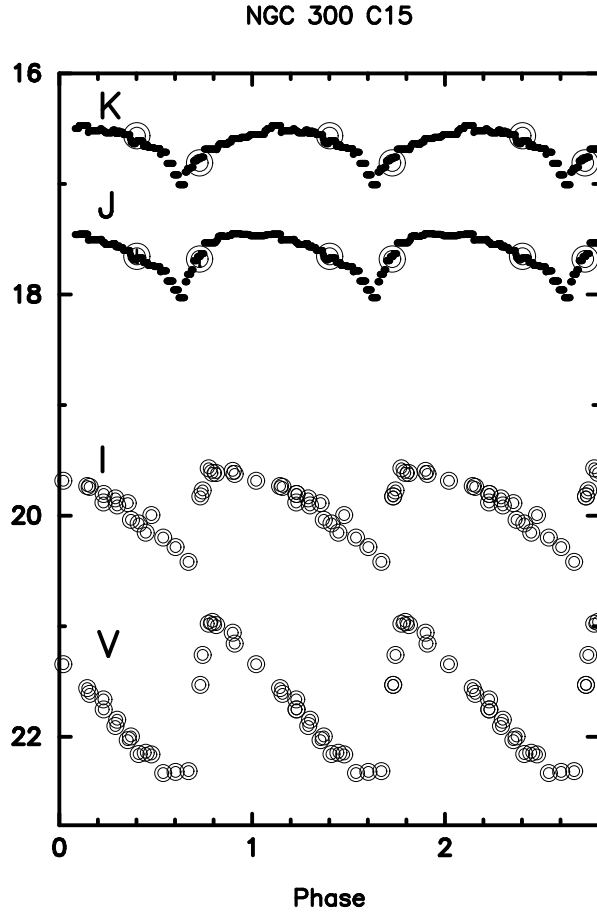


Fig. 7.— V and I light curves (lower half of the figure) for the 32-day extragalactic Cepheid C15 in NGC 300. The upper panel shows the CPR predictions based on V and I data (solid dots) for two near-infrared bandpasses (K & J) overlaid upon the only two random-phase observations (circled circles) available for this Cepheid. The size of the inner circle closely approximates the quoted errors on the near-infrared photometry. These data are well fit by the CPR predictions.

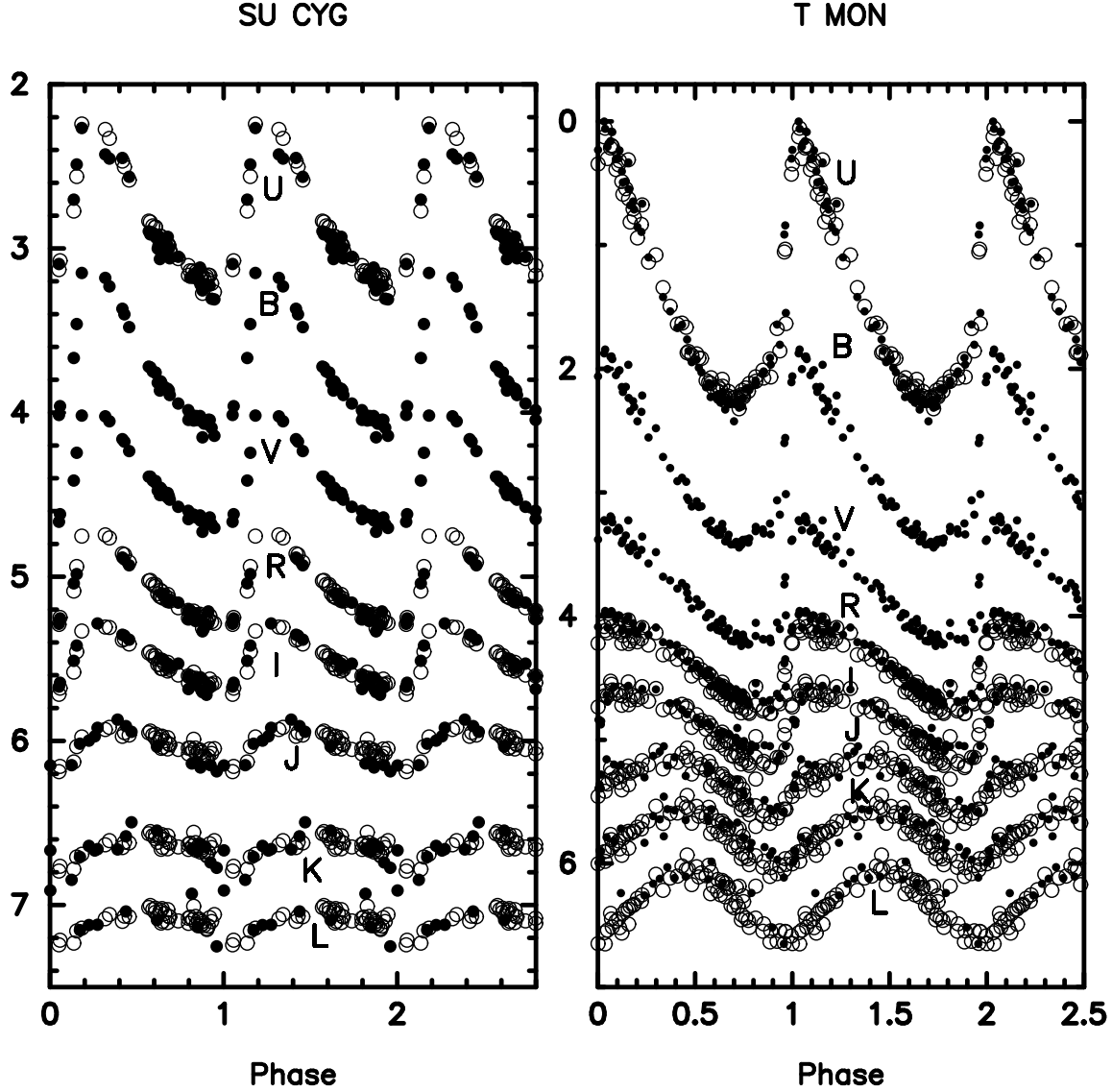


Fig. 8.— The two Cepheids, SU Cyg and T Mon, shown at the beginning of the article but now with their multi-wavelength light curves delineated by the original observations (filled circles) overlaid with CPR predictions (open circles) derived from the BV light curves alone. The noise in the predictions is directly ascribable to the photometric noise in the basis-generating B and V light curves.

## References

- Freedman, W. L. 1988, *ApJ*, 326, 691
- Gieren, W. et al. 2004, *AJ*, 128, 1167
- Gieren, W. et al. 2005, *ApJ*, 628, 695
- Imbert, M. 1981, *A&AS*, 44, 319
- Imbert, M. 1987, *A&A*, 175, 30
- Imbert, M. et al. 1985, *A&AS*, 61, 259
- Kanbur, S.M., & Mariani, H. 2004, *MNRAS*, 355, 1361
- Kervella, P., Bersier, D., Mourard, D., Nardetto, N., Fouque, P., & Coude du Foresto, V. 2004, *A&A*, 428, 587
- Labhardt, L., Sandage, A., & Tammann, G. A. 1997, *A&A*, 322, 751,
- Madore, B. F. 1985, *ApJ*, 298, 340
- Moffett, T.J., Giren, W.P., Barnes, T.G., & Gomez, M. 1998, *ApJS*, 117, 135
- Persson, S.E., Madore, B.F., Kzreminski, W., Freedman, W.L., Roth, M., & Murphy, D.C. 2004, *AJ*, 128, 2239
- Soszynski, I., Gieren, W., & Pietrzynski, G. 2005, *PASP*, 117, 823
- Stebbins, J. 1945, *ApJ*, 101, 47
- Tanvir, N.R., Hendry, M.A., Watkins, A., Kanbur, S. M., Berdnikov, L. N., & Ngeow, C. C. 2005, *MNRAS*, 363, 749
- Wisniewski, W.Z., & Johnson, H.L. 1968, *Comm. Lunar Planet. Lab.*, No. 112, 57
- Yoachim, P., McCommas, L.P., Dalcanton, J.J., & Williams, B.F. 2009, *AJ*, 137, 4697